



AIAA-2003-4258

Development of Closed-loop Control for Cavity Flows

M. Samimy, M. Debiasi, E. Caraballo

The Ohio State University
Department of Mechanical Engineering

H. Özbay, M. Ö. Efe, X. Yuan

The Ohio State University
Department of Electrical Engineering

J. DeBonis

NASA Glenn Research Center

J. H. Myatt

Air Force Research Laboratory
Air Vehicles Directorate

33rd AIAA Fluid Dynamics Conference and Exhibit
23-26 June 2003 / Orlando, Florida

Development of Closed-loop Control for Cavity Flows

M. Samimy, M. Debiase, E. Caraballo
 Gas Dynamics and Turbulence Laboratory
 Department of Mechanical Engineering
 The Ohio State University
 206 West 18th Avenue
 Columbus, Ohio 43210
 Samimy.1@OSU.edu

H. Özbay, M. Ö. Efe, X. Yuan
 Department of Electrical Engineering
 The Ohio State University

J. DeBonis
 NASA Glenn Research Center

J. H. Myatt
 Air Force Research Laboratory
 Air Vehicles Directorate

Abstract

Flow control is one of the main thrust areas of the Collaborative Center of Control Science (CCCS) at the Ohio State University. The primary objective of the flow control team at CCCS is to develop tools and methodologies for closed-loop flow control. The team possesses synergistic capabilities in all of the required multidisciplinary areas of flow simulation, low dimensional modeling, controller design, and experimental integration and implementation of the components along with actuators and sensors. The initial application chosen for study is closed-loop control of shallow cavity flows in subsonic Mach numbers. Shallow cavity flows have well known characteristics, are amenable to low dimensional modeling, possess known and localized receptivity, and are amenable to external forcing. Therefore, they are quite suited for closed-loop control technology development. The team has made significant progress in the development of various components necessary for low dimensional model based control strategy, which will be presented and discussed in this paper. The current experimental set up utilizes a titanium diaphragm compression driver for actuator, which is capable of forcing the flow up to about 10 kHz in the Mach number range of 0.25 to 0.5. While the low dimensional model based controller design is progressing steadily, a simple logic-based controller has been implemented, which can suppress the peak pressure fluctuations in the cavity up to 23 dB. The effectiveness of the controller is reduced at higher Mach number flows, presumably due to the lack of actuation authority.

1. Introduction

The flow control team at the Ohio State University (OSU) Collaborative Center of Control Science (CCCS) is working to develop tools and methodologies for closed-loop aerodynamic flow control. The team, composed of OSU, Air Force Research Laboratory, and NASA researchers, is taking a truly multidisciplinary approach from the outset by bringing together people with skills in experimental and computational fluid mechanics, reduced order modeling, control law design, sensor and actuator development, and applied mathematics to tackle this challenging problem in a coordinated fashion rather than in a piecemeal approach.

The team's ultimate goal is to enable the use of closed-loop aerodynamic flow control to control the flow over maneuvering air vehicles and ultimately to control the motions of the vehicles themselves. To that end, a systematic approach consisting of simulation, reduced-order modeling, control law design, and experimental validation was adopted. This is necessary to develop tools that will be generally useful, rather than developing a method that applies for one problem to be addressed by flow control but is less relevant for another.

The initial application chosen for study is closed-loop control of the large amplitude pressure fluctuations created by a shallow cavity flow (Samimy *et al.* 2003 and Caraballo *et al.* 2003). Cavity flows have well known

characteristics, are amenable to low dimensional modeling (*i.e.* dominated by coherent structures), possess known and localized receptivity, and are amenable to external forcing. The cavity problem has long been an attractive problem for researchers due to the rich nature of the flow physics and its relevance to practical applications (Rossiter 1964). Attempts to control the cavity flows using open-loop control, or methods that do not require feedback, have been successful at suppressing cavity tones at specific flow conditions (e.g. McGrath and Shaw 1996, Cain *et al.* 2000, Stanek *et al.* 2002a & b). The use of feedback can increase robustness to external disturbances and changes in flight conditions (Cabell *et al.* 2002, Rowley and Williams 2003, Rowley *et al.* 2001 & 2002, and Williams *et al.* 2002) and can potentially reduce actuator power requirements by an order of magnitude (Cattafesta *et al.* 1997). While several researchers have been successful at implementing closed-loop control of cavity flows, all of the efforts required extensive experimental testing for model development prior to control law design. In addition, many resulted in models that were based on the physical mechanisms that pertain specifically to cavity flows. As a consequence, the resulting techniques would be difficult to use for objectives other than the suppression of cavity tones. Toward that end, the CCCS flow control team is working to develop a systematic method for control of the tones created by subsonic flow over a shallow cavity. The ultimate goal is to develop methods for the closed-loop control of aerodynamic flows that could be extended to a wide variety of problems.

A systematic study of the level of fidelity required to accurately capture the flow physics was conducted to determine the appropriate level of computational complexity at which to carry out the needed simulations. While two-dimensional simulations allow the generation of results more quickly than three-dimensional simulations, some of the processes involving vortical structures are not properly modeled. As a result, quasi-three-dimensional simulations that allow for processes such as vortex-tilting and vortex-stretching while ignoring sidewall effects are being used to model the flow. Two-dimensional simulations are currently being used for preliminary modeling work in order to develop the tools that will be later used when the three-dimensional simulations become available. To date, two-dimensional simulations are complete for two baseline (no actuation) cases with Mach numbers 0.38 and 0.30, and for the forcing of the latter case by a synthetic jet at two different frequencies. In addition, a quasi-three-dimensional simulation for the second baseline case is underway.

With input from preliminary simulation data, an excellent experimental facility was constructed. The cavity has an adjustable depth to allow multiple configurations, although all data collected thus far are for

a square cavity of length-to-depth ratio of four. The flow spectra without actuation were characterized for Mach numbers ranging from 0.25 to 0.50, and the resonant frequencies correlate well with predictions by Rossiter (1964). A zero net-mass flow rate actuator, using a titanium diaphragm, is used to force the flow at the leading edge of the cavity, *i.e.* at the receptivity location of the shear layer spanning the cavity. As it will be discussed in Section 5 and is detailed in Debiasi and Samimy (2003), the actuator was characterized and found to be well suited for forcing in a broad range of frequencies and amplitudes. In addition, a logic-based controller was developed and used to demonstrate the experimental capability of applying feedback control.

Due to the large number of states in the computational fluid dynamics model of the cavity, a reduced order model of the flow is required. Until the quasi-three-dimensional simulations are complete, the two-dimensional data are being used as a test case. Proper orthogonal decomposition (POD) is being used in conjunction with Galerkin projection to produce a model for control law design. The model for some Mach numbers is well behaved, while stability issues arise for some other Mach numbers. Hence, stability issues are the current focus of the reduced order modeling effort.

Until a reduced order model is developed for control law design, several sample problems are being addressed. Control laws were designed for one- and two-dimensional heat flow and for one-dimensional Burgers' equation with an emphasis on the separation of the control input from the remainder of the spatial locations in the set of ordinary differential equations. In addition, the model of Rowley *et al.* (2002) based on the physical processes in cavity flows is being used for additional control law design work.

Progress made to date in each of the components discussed above will be presented below. More details of the experimental component are given in a companion paper by Debiasi and Samimy (2003).

2. Numerical Simulation

The primary objective of the simulation is to provide detailed flowfield data in order to develop a reduced-order model of the cavity using Proper Orthogonal Decomposition (POD) and Galerkin projection. Previously reported results (Caraballo *et al.* 2003) focused on developing an understanding of the consequences of various modeling approaches and assumptions. The goal of this prior work was to develop a methodology to produce accurate simulation data with the minimum required computational cost. Details of the numerical scheme, computational grid, and boundary conditions can be found in Caraballo *et al.* (2003), and only a summary will be given below.

First, the effect of using two-dimensional (2-D) versus three-dimensional (3-D) simulations was explored. It was shown that the two-dimensional simulations could not reproduce the pressure spectra found in the experimental results. By solving the 2-D version of the Navier-Stokes equations, the motion of turbulence structures in the fluid is restricted in such a way that it does not allow for vortex stretching and tilting. This resulted in very large structures in the cavity shear layer and modes with frequencies much lower than those observed in the experimental results. The 3-D simulations yielded much smaller and higher frequency structures in the cavity shear layer. The resulting pressure spectra accurately matched the experimental results (Samimy et al. 2003). To save computational cost, the 3-D simulations did not model the entire width of the cavity. Only a narrow span of the cavity was modeled with periodic boundary conditions used to allow for three-dimensional flow structures to develop and convect realistically. This simplification significantly reduced computational cost without adversely affecting accuracy.

Second, the effect of the state of the upstream boundary layer and its modeling was examined. The simulation is run on a very coarse grid relative to the turbulent scales in the upstream boundary layer. Without a turbulence model, the simulation produces a laminar boundary-layer. The use of a Baldwin-Lomax turbulence model (Baldwin and Lomax 1978) in the boundary layer upstream of the cavity was examined. A comparison of the laminar and turbulent 2-D simulations showed that the turbulent boundary layer did have some effect on the flowfield and resulting pressure spectra in the cavity. However, the effect was small compared to the difference between the 2- and 3-D simulation results. In addition, the turbulence model adversely affected the stability of the solution. The turbulent solution required a time step 10 times smaller than the laminar simulation. It was decided that the simulation would forgo turbulence modeling to reduce simulation time, a necessity for 3-D calculations.

Recent work has focused on the simulation of the actuator and the effect of forcing on the cavity flow. The actuator is a compression driver with a titanium diaphragm with zero net-mass flow rate located near the top of the upstream cavity wall - the receptivity region of the cavity shear layer. Detailed hot-wire measurements in the experimental facility (Debiasi and Samimy 2003), at the exit of the actuator were used to characterize the actuator output. It was determined that for the purposes of the simulation a sinusoidal variation of the velocity at the actuation frequency would be a reasonable representation. The actuator is simply modeled as a boundary condition imposed on the surface of the upstream cavity wall (Figure 2.1). Note that the grid has been magnified near the cavity entrance and the height of

the outlet of the actuator is only 1 mm. The amplitude, frequency, exit angle, and total temperature of the pulsing jet are specified. To account for the characteristic wave moving from the domain to the boundary in a simple manner, the density on the boundary is extrapolated from the interior grid points.

The 3-D simulations of the cavity are very time intensive but necessary for developing accurate low-order models. While the 3-D results are being computed, it was desired to have preliminary data to use for low dimensional model development and to evaluate the various processes involved. Even though the 2-D results do not match the experimental results, they are still valid solutions to the 2-D Navier-Stokes equations and can therefore be used for preliminary low dimensional modeling work. Three 2-D simulations were obtained for the Mach 0.3 flow: one for the baseline (unforced) case, and two for sinusoidal forcing with amplitude 20 m/s and frequency 1650 Hz and 2200 Hz. The actuator output is angled upward 30 degrees to the incoming horizontal flow. Surface static pressure data at the center of the cavity floor was sampled at 50 kHz. Figure 2.2 presents the power spectra of the pressure signal for the three cases using 2048 samples and a frequency range of up to 25 kHz and frequency resolution of about 12 Hz. Unlike in the experimental measurements, the averaging spectra over 50 or 100 blocks of data is not possible in the simulations and therefore these spectra are not smooth. However, normalizing the spectra with the amplitude of the baseline peak brings out the dominant peaks.

The baseline case (Figure 2.2a) shows that the cavity produces a very strong tone at 293Hz and a weaker one at its harmonic. The frequency of the primary peak is much lower than both the shear layer instability frequency of 2.1 kHz (obtained assuming a shear layer momentum thickness $\theta = 1$ mm and using $f\theta/U \sim 0.02$) and the first Rossiter mode of approximately 800Hz. Comparing this case with the actuated cases (Figures 2.2b & 2.2c) clearly shows that the actuator has a strong effect on the flowfield. First, a tone at the actuating frequency can be seen. But more importantly, both spectra with actuation have been significantly altered from the baseline case. Even though the modes in the baseline case are different than the Rossiter modes, the response of the flow seems to be quite similar to the experimental case (Williams *et al.* 2002); the result in Figure 2.2b is similar to “peaking” and in Figure 2.2c is similar to “peak splitting.” It should be noted that while these two phenomena were observed experimentally by changing the actuation amplitude, in this simulation the actuation amplitude is fixed, but the forcing frequency is changed.

From Figure 2.2 it is clear that the actuator, as implemented through the boundary condition, does significantly affect the flowfield. These results are being used to discern the effect of actuation on the corresponding POD modes and low dimensional models.

Three-dimensional simulations of the cavity with and without actuation are currently underway. These results will be validated against experimental data and then used to develop the low order model and resulting controller for the flow.

3. Low Dimensional Modeling

Fluid flows are governed by the N-S equations, which is a set of highly non-linear partial differential equations. Due to the need for very large computing power and storage for practical problems and the infinite dimensionality of these equations, they are not useful for feedback control purposes. Therefore, a key to successful implementation of closed-loop flow control is the development of simple flow models that can capture the essential dynamics of the flow upon which a controller can be based.

A well-known technique in the fluid dynamics community that can be used for deriving low dimensional models is the Proper Orthogonal Decomposition (POD). The method provides a spatial basis (a set of eigenfunctions) for a modal decomposition of an ensemble of data obtained from experiments or numerical simulations. The eigenfunctions, or modes, are extracted from the velocity fluctuations cross-correlation tensor, and can be used as basis functions to represent the flow. However, to go one step beyond the mere identification of these modes and to investigate their evolution with time, one needs to project the N-S equations (e.g. via Galerkin projection) onto these eigenfunctions to derive a set of ordinary differential equations (ODE) that can be used to reconstruct, at least in an overall sense, the behavior of the flow (e.g. Gordeyev and Thomas 2000, Smith *et al.* 2002).

In an earlier work from our team, the POD method was used to study the flow over a cavity using numerical simulation data for a baseline case with a Mach number of 0.38 (Caraballo *et al.* 2003). Two aspects of the low dimensional model development were investigated: the effect of the norm definition used for the inner product, and the convergence of the time coefficients obtained from a reduced system of ODEs, derived by projection of the governing equations onto the POD basis. For the cavity flow, it was observed that the shape of the POD modes as well as the amount of energy captured by each mode did not change significantly for the two different norms (a vector-valued and a scalar-valued norm). Also, four modes captured over 90% of the energy in the flow in either approach. When the Galerkin projection method was used, it was observed that with less than five POD modes the solution of the time coefficients obtained from the system of ODEs did not converge for either norm. Additionally, the time coefficients of the scalar-valued norm followed the original value only for one cycle after which they diverged regardless of the number of modes.

On the other hand, for the vector-valued norm as the number of modes was increased, improvements in the level and phase of the time coefficient were noticed, with the best results obtained using 8 to 10 modes. However, when more than 12 modes were used, the solution diverged. These results are in agreement with the results of Rowley *et al.* (2001), showing that, for the reconstruction of the flow dynamics in the case of compressible flow, an inner product defined by a vector norm produced better results than a scalar norm.

The current effort is on deriving a low dimensional model for different cases of external forcing applied to the flow and on how to represent the external forcing effect explicitly. This paper is a follow up of the work presented by Caraballo *et al.* (2003) where further details of the background of low dimensional modeling can be found. Below a brief background and some preliminary results will be presented and discussed.

3.1 POD Method

The POD method was introduced by Lumley (1967) to the fluid dynamics community as an objective way to extract large-scale structures in a turbulent flow. Details on the fundamentals of the POD method can be found in Berkooz *et al.* (1993) and Holmes *et al.* (1996). The general idea is to decompose the flow field into a set of orthogonal bases that contains the most dominant characteristics of the flow. To reduce computational requirements POD modes can be obtained from highly spatially-resolved data sets like those obtained from numerical simulations or advanced laser based diagnostics using the snapshot method, Sirovich (1987). The method requires a sufficiently large number, $k = 1, 2, \dots, M$, of time realizations for the instantaneous velocity field $\mathbf{u}(\mathbf{x}, t_k)$, with the realizations being uncorrelated at least over several snapshots. Then the POD eigenfunctions $\boldsymbol{\varphi}^n(\mathbf{x})$ can be written as linear combinations of the instantaneous flow field,

$$\boldsymbol{\varphi}^n(\mathbf{x}) = \sum_{k=1}^M \mathbf{A}_k \mathbf{u}(\mathbf{x}, t_k) \quad (3.1)$$

where \mathbf{A}_k is the matrix of time coefficients corresponding to the k^{th} time realization obtained by solving the intermediate eigenvalue problem,

$$\mathbf{C}(t, t_k) \mathbf{A} = \lambda^n \mathbf{A} \quad (3.2)$$

where λ^n is the eigenvalue. The two-point correlation tensor (\mathbf{C}) of independent snapshots integrated over the spatial domain of interest is defined as:

$$\mathbf{C}(t, t_k) = \frac{1}{M} \int_D \mathbf{u}(\mathbf{x}, t) \mathbf{u}(\mathbf{x}, t_k) \, d\mathbf{x} \quad (3.3)$$

This procedure reduces the eigenvalue problem from one that depends on the number of grid points to one that

depends only on the number of snapshots (M) or ensembles used. In this work the snapshot method is used to obtain the POD basis (Caraballo *et al.* 2003). Then the flow field can be reconstructed using the eigenfunctions, as:

$$\mathbf{u}(\mathbf{x}, t) = \sum_{n=0}^{N_{POD}} a^n(t) \boldsymbol{\varphi}^n(\mathbf{x}) \quad (3.4)$$

where N_{POD} is the number of POD modes to be used, and $a^n(t)$ are the time coefficients obtained by projecting the instantaneous realizations $\mathbf{u}(\mathbf{x}, t)$ of the flow field onto the empirical eigenfunctions $\boldsymbol{\varphi}^n(\mathbf{x})$ as follows:

$$a^n(t) = \int_D \mathbf{u}(\mathbf{x}, t) \bullet \boldsymbol{\varphi}^{n*}(\mathbf{x}) d\mathbf{x}. \quad (3.5)$$

Obviously, to calculate the random or temporal coefficients, the instantaneous flow field must be measured or numerically calculated simultaneously at every point in the flow domain of interest.

3.2 Galerkin Projection and Low Dimensional Model

In developing a low dimensional model, we are interested in estimating the flow evolution from a given state. We use the Galerkin projection method to derive a reduced system of ODEs from which the time coefficients $a^n(t)$ in Eqn. 3.5 and thus the evolution in time of the flow from an initial state can be estimated. The idea is to project the governing equations, the compressible N-S equations in this case, onto the POD basis. More precisely, the flow variables are first decomposed into their mean and fluctuating components. The latter are then substituted into the governing equations and the resulting expression is projected onto the POD basis by taking the inner product of each term with the basis, according to the specified norm (scalar-valued or vector-valued). The system of ODEs so obtained is then truncated at the number of desired modes.

Following Rowley (2002), we use a simplified set of compressible, isentropic N-S equations as governing equations, which for the vector-valued norm approach can be written as:

$$\begin{aligned} \frac{Dc}{Dt} + \frac{\gamma - 1}{2} c \nabla \cdot \mathbf{u} &= 0 \\ \frac{D\mathbf{u}}{Dt} + \frac{2}{\gamma - 1} c \nabla c &= \frac{\mu}{\rho} \nabla^2 \mathbf{u} \end{aligned} \quad (3.6)$$

where c is the speed of sound, ρ is the fluid density, μ is the viscosity and γ is the ratio of specific heats. After following all the steps and simplifications outlined above, the resulting system of differential equations for calculating the time coefficient has the form:

$$\dot{a}^k(t) = b^k + \sum_{j=1}^n (d^{jk} a^j) + \sum_{j=1}^n \sum_{m=1}^n (g^{jmk} a^j a^m) \quad (3.7)$$

where b , d and g are constant coefficients obtained from the Galerkin projection. The number of modes, n , to be used defines the final number of ODEs.

Several attempts to derive a low dimensional model that can be used for different flow/forcing conditions have been made. For example, Ukeiley *et al.* (2001) compared the POD modes obtained from different flow conditions with the modes obtained from a combined set of snapshots taken from all flow conditions under study. They concluded that the main characteristics of all the flow conditions were captured in the combined set and suggested that this set could be used as a basis for the development of a low dimensional model. Smith *et al.* (2002) used the same approach of stacking snapshots of different forcing conditions for the wake behind a cylinder to obtain a single POD basis, and compared the results of this set with the individual forced results. They noticed that the required number of modes for the stack case increased with the forcing frequency, when compared to the individual forced cases. Sirovich and Rodriguez (1987) showed that for the Ginzburg-Landau equation the basis obtained for a particular value of the parameter μ_0 could still be used to represent a region of the parameter space with a three mode approximation. Additional information on the subject can be found in Delville *et al.* (1998).

Our approach is to derive a low dimensional model for the system where the control input appears explicitly in the final equation of the model. As detailed in (Efe *et al.* 2003a and 2003b) and briefly discussed in the next section, one can define Γ as the vector of control input. Performing the Galerkin projection with the control or forcing input applied at a specific location of the cavity, the following system of ODEs is obtained:

$$\begin{aligned} \dot{a}^k(t) &= b^k + \sum_{j=1}^n (c^{jk} a^j) + \sum_{j=1}^n \sum_{m=1}^n (d^{jmk} a^j a^m) \\ &+ \langle e^k, \Gamma \rangle_{s1} + \sum_{j=1}^n \langle f^{jk}, \Gamma \rangle_{s1} a^j \end{aligned} \quad (3.8)$$

The constant coefficients b , c , d , e and f are obtained from the Galerkin projection, as was done in the baseline case, and Γ is the control input applied at the forcing location.

Due to a convergence problem encountered in the solution of the system of ODEs obtained from the Galerkin projection for the Mach 0.3 baseline and forced cases, an alternative approach is also being investigated. The method is based on a least square fitting of the constant coefficients of the resultant system of ODEs for

the time coefficients and has been used by Gilles (1995) and Cohen *et al.* (2003) with good results when using only a low number of POD modes. The idea is to use the known form of the system of ODEs, equations 3.7 or 3.8, and to obtain the time coefficients by projecting the instantaneous velocity field onto the POD basis to find the best approximation of the constant coefficients b , c , d , e and f . Then the first step is to fit the known time coefficients with a cubic spline and calculate their time derivatives. Replacing these values into equation 3.7 the only unknowns left are the constant coefficients. Using all the time steps available the resultant system will have more equations than unknowns. Therefore the system is over determined and can be solved by the least square method. For more details on the procedure see appendix A on Gilles (1995). Furthermore, Gilles (1995) added some cubic terms to the quadratic model (Eqns. 3.7 and 3.8) to improve the solution without increasing the number of modes

3.3 Preliminary Results

Figure 3.1 shows the percent of energy recovered versus number of modes for the baseline case of $M = 0.38$, the baseline case of $M = 0.3$, the two forced cases at 1650 Hz and 2200 Hz for the latter flow, and for a combination of snapshots from the last three cases. To capture 90% of the energy, one needs only three modes in the $M = 0.38$ case and about nine modes in all other cases. Also, it seems that the higher frequency forcing slightly improves the amount of energy captured per number of modes while the lower frequency forcing worsens it. The combination case closely follows the lower frequency forcing case.

Figure 3.2-3.5 shows the first four POD modes for the four different cases (two baseline and two forced cases). As expected, the modes for the two baseline cases are quite different. For all the cases the modes seem to appear in pair in terms of the amount of energy content and also the size of structures, in agreement with the results of Rowley *et al.* (2001). In the two forced cases, some differences in the shape of the modes can be observed, where some of the structures seem to have been stretched or tilted, but there are no major changes in the energy content. The modes for the combined case (not shown here) seem to capture the main characteristics of all three cases used to form the combination.

Figure 3.6 shows the time coefficient obtained from the system of ODEs for $M = 0.38$ case (Caraballo *et al.* 2003). For this case there is convergence in the solution when the number of modes used ranges between five and twelve - best results are obtained when 8 or 10 modes are used. Increasing the number of modes beyond ten does not show any appreciable improvement in the solution, which in most of the cases starts to deviate substantially from the original values after four or five cycles. Similar results have been cited by other researchers (Rowley *et*

al. 2001). While intuitively one would think that increasing the number of modes would improve the results, apparently there is no mathematical basis for such a trend (Burns 2002). In the case of $M = 0.3$ flow, up to this point the system of equations has shown an unstable behavior for any number of modes used. The cause of this problem is currently being investigated.

Figure 3.7 shows a comparison of the first time coefficient calculated with the Galerkin projection and the least square approximation with the original value, for the case of $M = 0.38$. It can be noticed that, when the Galerkin projection was used, the solution did not converge to the original value. When only quadratic terms were used in the least square method the solution did not improve much. Finally when the cubic terms involving the first two time coefficients were included (Cubic2) the solution converged to the original value, showing only a small phase shift after several cycles. For the case of $M = 0.3$ (not shown here), although the solution is stable it diverges from the original values of the time coefficients. This issue is currently being investigated. The main difference between $M = 0.38$ and $M = 0.3$ is that the former is characterized by a single-mode with robust structures and quite periodic behavior for the time coefficient while the latter has multiple modes with a pseudo-periodic and more random behavior.

While the issues discussed above are being investigated, we are using two different approaches in the development of the low dimensional model for the controller design. In the first approach, individual basis for each case as well as for a composed set, where all the baseline and forced cases for the $M = 0.3$ flow are being used by stacking different snapshots, are obtained with its corresponding system of ODE's. In the second approach the control input in a small region (or point) is separated from the rest of the domain, and thus appears explicitly in the resulting system of equations. As it will be discussed in the next section, this is the preferred system and will be used in the design of the controller.

4. Controller Design

The low dimensional model, which is developed by using POD and Galerkin projection as discussed above, represents the "plant" in the closed loop control scheme. When the coefficients in (Eqn. 3.7) are calculated, it becomes apparent that the corresponding system of ODEs is specific to a set of particular experimental or simulation conditions for which the coefficients have been determined, and the model (Eqn. 3.7) carries the effect of the boundary excitation/control input implicitly. However, to design and implement a controller, the boundary excitation must be identified explicitly. In the following, we describe a way to handle this problem. The emphasis of this section is to show how a transition from

an experiment-specific/simulation-specific set of ODEs to a more generally descriptive input-equipped model is established.

4.1 Control Oriented Modeling

As discussed in Section 3 of the paper, POD is a mathematical technique that uses spatial correlations obtained experimentally or numerically to extract the modes that contain the most significant dynamics of the flow. The scheme yields a set of orthonormal basis functions with a set of associated temporal coefficients. The N-S equations are then projected onto these basis functions using the Galerkin projection to obtain a set of ODEs, which characterize the flow under a set of conditions over which the spatial correlations were obtained. An important part of the dynamical system for controller design is the boundary excitation or the control/forcing input. It is not obvious how to incorporate this control input into POD based ODEs. More precisely, application of the Galerkin projection to a POD model yields an *autonomous* set of ODEs (consisting of only the state variables), which does not illustrate the effect of the control input (i.e. the boundary excitation). Therefore, this model does not explicitly describe the input/state/output behavior of the plant to be controlled. In what follows, we discuss a generic method to separate the effect of boundary excitation from the remaining terms of the POD based model so that it appears in the set of ODEs as an external input that we can manipulate by the feedback controller. As before, boldface symbols are used to denote vector quantities.

Let us define S_2 as the physical location/region at which the boundary excitation or flow forcing enters, and S_1 as the remainder of the domain of interest. The overall physical domain is then $S := S_1 \cup S_2$. A discrete representation of S denoted by S_D is used. The algorithmic schemes are computed over S_D (the grid) that matches the simulation or the experimental data over the physical space. This idea naturally brings us to work on partitioned subsets to capture the effect of the forcing input boundary condition and its effect over the spatial domain individually. A precise mathematical derivation of this procedure is given below.

Consider a process characterized by the partial differential equation

$$\mathbf{q}_t(S, t) = \mathbf{f} \left\{ \begin{array}{l} \mathbf{q}(S, t), \mathbf{q}_x(S, t), \mathbf{q}_y(S, t), \\ \mathbf{q}_z(S, t), \mathbf{q}_{xx}(S, t), \dots \end{array} \right\}, \quad (4.1)$$

where \mathbf{q} is a generic vector of flow variables that are functions of space and time with the subscripts denoting the derivatives with respect to the corresponding variables. Assume that the equation above admits a unique solution, which can be expressed as

$$\mathbf{q}(S, t) = \mathbf{q}_m(S) + \sum_{i=1}^M a^i(t) \boldsymbol{\varphi}^i(S) \quad (4.2)$$

where \mathbf{q}_m , a_i and $\boldsymbol{\varphi}_i$ denote the mean flow variables, the i -th temporal component, and the i -th spatial basis, respectively. Noting that the process takes place over the physical domain S , and inserting the above solution in equation 4.1 yields

$$\sum_{i=1}^M \dot{a}^i(t) \boldsymbol{\varphi}^i(S) = \mathbf{f} \left\{ \left[\mathbf{q}_m(S) + \dots \right], \frac{\partial}{\partial x} \left[\mathbf{q}_m(S) \dots \right], \dots \right\} \quad (4.3)$$

$$:= \mathbf{f}\{S, t\}$$

Taking the inner product of both sides with $\boldsymbol{\varphi}^k(S)$ results in

$$\dot{a}^k(t) = \langle \boldsymbol{\varphi}^k(S), \mathbf{f}\{S, t\} \rangle, \quad k=1, 2, \dots, M. \quad (4.4)$$

The key here is to notice that $\langle \boldsymbol{\varphi}^k(S), \mathbf{f}\{S, t\} \rangle = \langle \boldsymbol{\varphi}^k(S_1), \mathbf{f}\{S_1, t\} \rangle + \langle \boldsymbol{\varphi}^k(S_2), \mathbf{f}\{S_2, t\} \rangle$ holds true by the definition of the inner product. Clearly, the above partitioning corresponds to calculating an integral over two domains, the union of which gives the original domain of the problem while the intersection is obviously an empty set. This significantly influences the dynamical representation of the set of ODEs, which now turn out to be

$$\dot{a}^k(t) = \langle \boldsymbol{\varphi}^k(S_1), \mathbf{f}\{S_1, t\} \rangle + \langle \boldsymbol{\varphi}^k(S_2), \mathbf{f}\{S_2, t\} \rangle, \quad k=1, 2, \dots, M. \quad (4.5)$$

When the above inner products are calculated over the discrete sets S_{D1} and S_{D2} , the latter referring to the control location, the final equation can be rewritten as

$$\dot{a}^k(t) = \langle \boldsymbol{\varphi}^k(S_{D1}), \mathbf{f}\{S_{D1}, t\} \rangle + \langle \boldsymbol{\varphi}^k(S_{D2}), \mathbf{f}\{S_{D2}, t\} \rangle, \quad k=1, 2, \dots, M. \quad (4.6)$$

This equation contains sufficient degrees of freedom to derive an analytic model. This is because the suggested solution must be satisfied at S_{D2} , and this makes the term $\langle \boldsymbol{\varphi}^k(S_{D2}), \mathbf{f}\{S_{D2}, t\} \rangle$ computable by utilizing the boundary excitation denoted by Γ explicitly. Depending on the form of the vector function \mathbf{f} , the procedure described will yield a non-autonomous set of ODEs capturing the dynamics in the following form:

$$\dot{\mathbf{a}}(t) = A(\mathbf{a}) + B(\mathbf{a})\Gamma \quad (4.7)$$

From this point on, the control objectives can be put forward. The achievability of these objectives will strictly

be dependent upon the content of the vector functions A and B described as

$$A(a) = \tilde{F} + \tilde{G}a + a^T \tilde{H}a \quad (4.8)$$

$$B(a) = \tilde{P} + \tilde{Q}a \quad (4.9)$$

The calculation of the tilde-terms seen above is straightforward yet tedious. For a detailed treatment of the control separation technique as applied to simpler systems, the reader is referred to Efe and Özbay (2003a and 2003b). The underlying idea is to manipulate the grid points around external excitation separately (refer to (4.6)): the solution there is independently specified; yet, it has to satisfy the Navier-Stokes equations. As a result, the control inputs appear explicitly in the last term of (4.6). In what follows, the frequency dependence of the model in (4.7) is discussed.

4.2 Controller Design and Frequency Dependence of POD Models

The design of a controller closing the loop with the needed excitation signals depends heavily on how well the model describes the physical system. The frequency dependence of POD based models is a fundamental issue from this point of view (Efe and Özbay 2003a). Although the problem can be remedied at the cost of dealing with more complex models, the ultimate form of the dynamics will admit the form given in equations (4.7)-(4.9).

Given the temporal dynamics (4.7), the control engineering expertise offers a set of approaches depending on the objectives (Slotine and Li 1991, Isidori 1995, Aström and Wittenmark 1992). These include -but are not limited to- feedback linearization, adaptive control, optimal control, expert control (Jang *et al.* 1997), or hybrid variants of them.

The work towards the dynamical system modeling is in progress, and systematic approaches for controller design are underway.

4.3 An Alternative Modeling Viewpoint and Approach to Controller Design

Although research in closed-loop flow control is mostly dominated by decomposition-based model construction, a different approach has recently focused on the development of a physics based model (Williams *et al.* 2002, Rowley *et al.* 2001, and Rowley *et al.* 2002). In this approach, the fundamental physical processes in a cavity flow (e.g. shear layer instability, acoustic scattering, etc.) are represented by transfer function models. One advantage of a model devised with this approach is that the model is parameterized. Such flexibility is useful for capturing important flow features with a time varying set of parameters. Our work has shown that the H_∞ control synthesis technique of Toker

and Özbay (1995), developed for a class of infinite dimensional systems, is applicable to the models introduced by Rowley *et al.* (2001, 2002).

In Yuan *et al.* (2003), it is demonstrated that the H_∞ controller for delay based models is useful particularly in suppressing the undesired tones in the frequency response of pressure fluctuations, which are observed from a sensor located at the center floor of the cavity. The paper fits a model to the simulation data of Navier-Stokes equations and presents the controller design in detail.

Current research on the real-time implementation of the controller described in Yuan *et al.* (2003) in a cavity flow experiment (Debiasi and Samimy 2003) is in progress. Several issues need to be addressed in order to assess the performance of the controller. These include numerically robust implementation of the controller, on-line parameterization of the flow dynamics, and modeling of actuator.

5. Experiments

In this section we briefly discuss the experimental activities and present the experimental results obtained up to date at the OSU Gas Dynamics and Turbulence Laboratory (GDTL) by the CCCS flow-control team. A small subsonic wind tunnel with a shallow cavity has been built and tested. The flow field in the Mach number range 0.25-0.5 has been explored. The tunnel in the current arrangement can operate continuously up to Mach 1. By replacing its converging nozzle with a converging-diverging nozzle, the facility can operate continuously in the supersonic regime. A synthetic-jet type actuator with a large bandwidth is used to force the shear layer at its receptivity region. A preliminary study of the effect of the actuation frequency on the Mach 0.3 flow has been conducted. While working on the development of a low dimensional model based controller, an initial logic-based controller has been implemented that searches in a closed-loop fashion the frequencies that reduce the cavity-flow resonant peaks. The technique has performed well in the experimental trials and has allowed identification of optimal frequencies for the reduction of resonant peaks in the Mach number range explored.

The flow facility, baseline flow characteristics, actuator behavior, effects of forcing on the flow, and finally the results obtained with the logic-based feedback control will be briefly presented and discussed. Details of the work can be found in Debiasi and Samimy (2003).

5.1 Flow facility

A modular, optically accessible experimental facility has been designed and fabricated at the Gas Dynamics and Turbulence Laboratory (GDTL) at The Ohio State University. The facility is of the blow-down type and operates with air supplied by two four-stage compressors.

The air is filtered, dried, and stored at 16.5 MPa in two high-capacity tanks. The air is conditioned in a stagnation chamber before entering the test section through a smoothly contoured converging nozzle. The total pressure in the stagnation chamber can be controlled within 0.07% of the test section static pressure (near ambient pressure). The cross-section of the test section is square with width $W = 50.8$ mm (2 in). The high of the upper wall of the test section is adjustable to compensate for the growth of the boundary layer and of the shear layer. A variable depth cavity that spans the entire width of the test section is recessed in the floor. In the current experiments, the cavity depth D is 12.7 mm (1/2 in) and its length L is 50.8 mm (2 in) for an aspect ratio $L/D = 4$. A schematic of the test section with the cavity and the actuator is shown in Fig. 5.1. Large optical windows and numerous ports allow the use of advanced imaging diagnostics as well as an array of transducers for pressure and velocity measurements. The facility allows continuous operation in the subsonic range with the current converging nozzle, but can easily be adapted to supersonic operation by changing this nozzle with a converging-diverging one.

The actuator is a 2D synthetic jet issuing from an high-aspect-ratio converging nozzle embedded in the cavity leading edge as shown in Fig. 5.1. The jet exhausts at an angle of 30° with respect to the main flow through a slot of width $W = 50.8$ mm (the cavity span) and height $h = 1$ mm. Actuation is provided by the movement of the titanium diaphragm of a Selenium D3300Ti compression driver whose voltage signal is amplified by a Crown D-150A amplifier. The compression driver diaphragm is capable of oscillating in the frequency range 1-20 kHz. In the rather unconventional arrangement of our experiments, where the compression driver is connected to a highly-converging nozzle, we expect a non-linear behavior as will be briefly discussed.

5.2 Baseline flow characteristics

Preliminary static and dynamic measurements of the flow characteristics have been carried out. Measurements of the static pressure at various locations were used to adjust the upper wall so to maintain a uniform pressure close to the ambient value along the test section. Flow velocity profiles were measured using a miniature pitot probe (0.8 mm tip diameter) traversing the test section in the horizontal and vertical planes 6.35 mm (1/4 in) upstream of the cavity leading edge. The boundary layer thickness at this location is about 2.5 mm both in the vertical and in the horizontal planes and follows a $1/n$ power law profile with $n = 6$. The flow outside of the boundary layer is very uniform across the test section. The Reynolds number based on the cavity step height is 10^5 and based on the incoming boundary layer thickness is 2×10^4 . Further details on the quality of the flow can be found in Samimy *et al.* (2003).

A complete survey of the cavity-flow resonance in the Mach range 0.25-0.5 was performed using a Kulite XTL-190-25A dynamic pressure transducer with frequency response up to 50 kHz flush-mounted in the middle of the cavity floor (Fig.5.1). The corresponding voltage signal was sampled at 200 kHz through a National Instruments PCI-6036E board installed on a Dell Dimension 8200 computer. The signal was band-pass filtered between 200 Hz and 20 kHz to remove spurious frequency components and converted to non-dimensional pressure value relative to the reference pressure 20 μ Pa. Then Sound Pressure Level spectra were derived.

The predicted Rossiter modes for our setup with L (the cavity length) = 50.8 mm, the ε (the phase lag parameter) = 0.25, and β (the ratio of the convective velocity to the freestream velocity) = 0.66 are presented in Figure 5.2 as a function of the flow Mach number. Small circles in the figure represent the frequency of the resonant peaks measured in our experimental setup. More specifically, closed circles represent dominant peaks, while open circles represent other peaks appearing in multi-mode resonance. The experimental setup exhibits strong, single-mode resonance in the Mach number ranges 0.25-0.31 and 0.39-0.5, and multi-mode resonance in the Mach range 0.32-0.38. The pressure spectra at Mach numbers 0.26 and 0.37 shown in Fig. 5.3 illustrate this point more clearly. Consistent with the observations of Cattafesta *et al.* (1998), it seems that in multi-mode resonance the energy available for generation of the acoustic tones had been split among the rapidly alternating peaks instead of concentrating on a single large peak.

5.3 Actuator behavior

Limited velocity measurements at the exit slot of the actuator without and with the main flow have been performed using a subminiature hot-film probe. Measurements were made without and with a main Mach 0.3 flow by placing the probe in the middle of the exit slot, *i.e.* at equal distance between the upper and the lower actuator outlet lips. To verify the spanwise uniformity of the jet, measurements were done at the test-section centerline (*i.e.* 1 in away from both the side-walls) as well as closer to the side-wall but outside the boundary layer (0.25 in from the wall). No difference has been detected between the center and side measurements both without and with the main flow. Figures 5.4 and 5.5 show the velocity at the actuator exit in terms of time and frequency, respectively, for no flow case. Figure 5.4 shows the velocity time traces at the exit slot for excitation at 1.6 kHz with 5 V_{rms} excitation voltage. The results with the Mach 0.3 main flow are very similar (Debiasi and Samimy 2003). Similar time traces were observed at the other actuation frequencies with

velocity values varying with frequency and decreasing at lower excitation voltages. Figure 5.4 also shows that, although the hot film records absolute velocity values, there is no indication of zero-velocity crossing. That is, apparently no negative velocity component is recorded in the middle of the exit slot. In fact the overall behavior resembles that recorded by Smith and Glezer (1998) immediately downstream of the exit slot of a piezoelectric-driven synthetic jet where the jet has already lost the sinusoidal momentum fluctuations occurring at the nozzle and exhibits a positive net momentum with peak instantaneous velocities 2-3 times the average one.

Figure 5.5 shows the variation of the peak and mean velocity at the exit slot as function of the actuation frequency for excitation at $5 V_{rms}$ without the main flow. As expected the actuator behavior is significantly non-linear with several peaks and valleys in the explored range of 1-10 kHz. This confirms the preliminary observations of non-linear behavior reported by Samimy *et al.* (2003) based on measurements of the forcing flow mean velocity obtained with the miniature pitot probe. The peak velocity values in excess of 20 m/s and the mean velocity values above 5 m/s shown in Figure 5.5 at some frequencies compare well with those observed by Chen *et al.* (2000) and by Guy *et al.* (2002) using high aspect ratio rectangular synthetic jets. The addition of the Mach 0.3 flow in the test section does not affect the behavior of the actuator.

5.4 Effect of forcing on Mach 0.3 cavity flow

In a series of experiments the actuator voltage was adjusted with the varying frequency to isolate the influence of frequency from that of amplitude and to maintain, as much as possible, a constant mean velocity of about 5 m/s at the forcing slot. The baseline Mach 0.3 cavity-flow spectrum is characterized by a single resonant peak of 132 dB at 2800 Hz (thin line in Figure 5.6). The forcing frequency was varied from 2 kHz to 10 kHz and complex response dynamics were observed. The response varied from; 1) a significant reduction in the baseline resonance peak with addition of a significant peak at the forcing frequency, 2) to reinforcement of the baseline resonance peak, 3) to a significant reduction in the resonance peak without adding new peaks. Figure 5.6 presents two forced cases (thick line) in comparison with the baseline case, illustrating the first and the third behaviors, respectively. With forcing at 2000 Hz, Figure 5.6 (a), the resonant peak is suppressed while a strong peak appears at the actuation frequency, an indication that the natural feedback has been interrupted and the system has been tuned to the actuator frequency. Figure 5.6 (b) shows the spectrum for actuation at 3250 Hz where the resonant peak is reduced by 18 dB without introducing a strong peak at the actuation frequency. Details of these results, which are consistent with the

results in the literature (*e.g.* Cattafesta *et al.* 1997, Williams *et al.* 2000, Cabell *et al.* 2002), are presented in Debiasi and Samimy (2003).

5.5 A simple logic-based feedback control

As was described above, various members of the team working on different components of the low dimensional model based feedback control are making steady progress. The experimental work, which is a part of the overall activities, will implement and evaluate the model-based controller. Meantime, we have developed a preliminary logic-based feedback control to test the experimental capabilities and to provide additional results on cavity flow control. An automated online routine was developed that continuously reads the cavity pressure/acoustic, determines its spectral distribution, then finds the actuation frequencies, if any, for which the spectral peak were eliminated or reduced by a specified value. If no major changes occur in the flow, the actuation is kept on at the optimum forcing frequency for spectral peak reduction. If there is a major change in the flow (*e.g.* a change in the Mach number in the range of 0.25 to 0.5 in the current set up) that affects the spectral characteristics, the actuation is automatically updated to achieve the set goal of reducing the peak amplitude by a certain level.

While this approach can hardly be classified as a closed-loop control scheme according to the established control theory, it nevertheless performed remarkably well as it was able to find and maintain forcing frequencies reducing strong cavity-flow resonant peaks in the whole range of Mach number explored. It also proved to be a powerful tool for extracting valuable information in a large range of flow and forcing conditions. In addition, this exercise showed that the experimental facility is ready for the implementation of various controller designed by our team or by other researchers working on the subject area.

In Figure 5.7 the solid line captures the "optimal" frequencies with actuator excitation voltage of $5 V_{rms}$ while the circles, similar to Figure 5.2, represent the original flow resonant frequencies for cavity flow Mach number of 0.25 to 0.5. Sometimes more than one forcing frequency exists for which a significant peak reduction is achieved. The "optimal" indicates the case for which the largest reduction has been observed. Based on the results presented in this figure, a simple controller can be derived that, at each Mach number, forces the flow at the optimal frequency for peak pressure reduction.

Figure 5.8 compares the highest values of the spectral peak as a function of the Mach number for the unforced resonant flow and for flow with optimal frequency forcing at $5 V_{rms}$ actuator excitation voltage. The thin line refers to the unforced case while the dotted line represents the intensity of the low-frequency noise plateau (*i.e.* the broadband pressure fluctuations at

frequencies below 1 kHz in Figure 5.3). The thicker solid line refers to the forcing case. These results show that optimal frequency forcing eliminates altogether the resonant peaks in the Mach 0.25-0.4 range. The resulting flow is so devoid of any significant peak that the maximum spectral level basically drops to the low-frequency noise plateau level. At higher Mach numbers, especially above Mach 0.45, the original resonant peak is much stronger and the optimal actuation is capable of producing a peak reduction of 10 dB. This is most probably due to the limitation of the actuator. It is also important to note that forcing produces little benefit at Mach numbers for which low-intensity peaks at multi-mode resonance exist (e.g. Mach 0.32) as the system is already in a state comparable to that induced by the actuation at optimal frequency.

6. Concluding Remarks

The primary goal of the flow control team at the Ohio State University Collaborative Center of Control Science is to develop tools and technologies for closed-loop aerodynamic flow control enabling the control of flow over maneuvering air vehicles and ultimately the control of the motions of the vehicles themselves. The team, composed of OSU, Air Force Research Laboratory, and NASA researchers, is taking a truly multidisciplinary approach by bringing together people with skills in experimental and computational fluid dynamics, reduced order modeling, control law design, sensor and actuator development, and applied mathematics to tackle from the outset this challenging problem in a coordinated fashion. The initial application chosen for study is closed-loop control of the large-amplitude pressure fluctuations created in a shallow subsonic cavity flow. Shallow cavity flows have well known characteristics, are amenable to low dimensional modeling, possess known and localized receptivity, are amenable to external forcing, and therefore, well suited for technology development. The cavity flow has long been an attractive problem for researchers due to the rich nature of the flow physics and its relevance to practical applications.

The coordinated efforts undertaken by the team include numerical simulation of the cavity flow; development of low order model of the flow using data from simulation results; design of a controller using the low-order model of the flow; and finally an experimental effort evaluating the simulation results and implementing and testing the overall control scheme. Significant progress has been made in all components. In the simulation work, a systematic study of the level of fidelity required to accurately capture the flow physics was conducted to determine the appropriate level of computational complexity at which to carry out the needed simulations. While two-dimensional simulations allow the generation of results more quickly than three-

dimensional CPU-intensive simulations, some of the processes involving vortical structures are not properly modeled. As a result, quasi-three-dimensional simulations that allow for processes such as vortex-tilting and vortex-stretching while ignoring sidewall effects are being used to model the flow. Two-dimensional simulations are being used for preliminary modeling work in order to develop the tools that will be used with the three-dimensional simulation results when they become available. To date, two-dimensional simulations are complete for two baseline (no actuation) cases with Mach numbers 0.38 and 0.30, and, with the latter flow, for two cases with actuation by a synthetic jet at two different frequencies. In addition, a quasi-three-dimensional simulation for the second baseline case is underway.

The computational fluid dynamics model of the cavity includes a large number of states, which makes it less useful for the design of a controller. Therefore, a reduced order model of the flow is required. Until the 3-D simulations are complete, results from the two-dimensional data are being used to provide the spatial correlation tensors required by proper orthogonal decomposition technique in conjunction with Galerkin projection to produce a model for control law design. While the model for some Mach number cases is well behaved, stability issues arisen in some other Mach number cases are currently the focus of the reduced order modeling effort.

Until a reduced order model is developed for control law design, several sample problems are being addressed. Control laws were designed for one- and two-dimensional heat flow and for one-dimensional Burgers' equation with an emphasis on the separation of the control input from the remainder of the spatial locations in the set of ordinary differential equations. In addition, an extended physics based model of Rowley *et al.* (2002) and other simple models are currently being used for additional control law design work.

With input from preliminary simulation data, an excellent experimental facility with adjustable cavity height and adjustable upper wall to achieve constant test section pressure has been constructed. All data collected thus far are for a square cavity of length-to-depth ratio of four. The flow facility has been evaluated and is well behaved where the resonant frequencies correlate well with Rossiter modes for Mach numbers ranging from 0.25 to 0.50. A compression driver with zero net-mass flow rate is used to force the flow at the leading edge of the cavity, the receptivity location of the shear layer spanning the cavity. The actuator was characterized and found to be well suited for this application in a broad range of frequencies. While the low dimensional model based controller design is progressing steadily, a simple logic-based controller has been implemented, which can suppress the peak pressure fluctuations in the cavity up to

23 dB. The effectiveness of controller is steadily reduced at Mach numbers above 0.4, presumably due to the lack of actuation authority. Details of the experimental work can be found in Debiasi and Samimy (2003).

Acknowledgements

The support of this work by the AFRL/VA and AFOSR through the Collaborative Center of Control Science (Contract F33615-01-2-3154) and by DAGSI is very much appreciated. The simulation work is supported in part under NASA Glenn's Aerospace Propulsion and Power Base Research and Technology Program and in part by a grant of computer time from the DOD High Performance Computing Modernization Program at the Army Research Laboratory. We thank Drs. Tom McLaughlin, Stefan Siegel, Kelly Cohen, Clancy Rowley, David Williams, and Larry Ukeiley for fruitful discussions.

References

- Aström, K.J. and Wittenmark, B., *Adaptive Control*, Prentice Hall, 1992.
- Baldwin, B. S., and Lomax, H., "Thin-Layer Approximation and Algebraic Model for Separated Turbulent Flows," AIAA Paper 78-257, January 1978.
- Berkooz, G., Holmes, P., and Lumley, J. L., "The Proper Orthogonal Decomposition in the Analysis of Turbulent Flows," *Annual Review of Fluid Mechanics*, Vol. 25, 1993, pp. 539-575.
- Burns, J., private communication, November 2002.
- Cabell, R. H., Kegerise, M. A., Cox, D. E., and Gibbs, G. P., "Experimental Feedback Control of Flow Induced Cavity Tones," AIAA Paper 2002-2497, June 2002.
- Cain, A. B., Rubio, A. D., Bortz, D. M., Banks, H. T., and Smith, R. C., "Optimizing Control of Open Bay Acoustics," AIAA Paper 2000-1928, June 2000.
- Caraballo, E., Samimy, M., and DeBonis, J., "Low Dimensional Modeling of Flow for Closed-Loop Flow Control," AIAA Paper 2003-0059, January 2003.
- Cattafesta, L. N., III, Garg, S., Choudhari, M., and Li, F., "Active Control of Flow-Induced Cavity Response," AIAA Paper 97-1804, June-July 1997.
- Cattafesta, L. N., III, Garg, S., Kegerise, M. A., and Jones, G. S., "Experiments on Compressible Flow-Induced Cavity Oscillations," AIAA Paper 98-2912, June 1998.
- Chen, F.-J., Yao, C., Beeler, G. B., Bryant, R. G., and Fox, R. L., "Development of Synthetic Jet Actuators for Active Flow Control at NASA Langley," AIAA Paper 2000-2405, June 2000.
- Cohen, K., Siegel, S., McLaughlin, T., and Myatt, J., "Proper Orthogonal Decomposition Modeling of a Controlled Ginzburg-Landau Cylinder Wake Model," AIAA Paper 2003-1292, January 2003.
- Delville, J., Cordier, L., and Bonnet, J. P., "Large-Scale-Structure Identification and Control in Turbulent Shear Flows," In *Flow Control: Fundamentals and Practice*, edited by Gad-el-Hak, M., Pollard, A., and Bonnet, J., Springer-Verlag, 1998, pp. 199-273.
- Debiasi, M. and Samimy, M., "An Experimental Study of the Cavity Flow for Close-Loop Flow Control," AIAA Paper 2003-4003, June 2003.
- Efe, M.Ö. and Özbay, H., "Proper Orthogonal Decomposition for Reduced Order Modeling: 2D Heat Flow," to appear in the Proc. of IEEE Int. Conf. on Control Applications (CCA'2003), June 23-25, Istanbul, Turkey, 2003a.
- Efe, M.Ö. and Özbay, H., "Integral Action Based Dirichlet Boundary Control of Burgers' Equation," to appear in the Proc. of IEEE Int. Conf. on Control Applications (CCA'2003), June 23-25, Istanbul, Turkey, 2003b.
- Gillies, E. A., "Low-Dimensional Characterization and Control of Non-Linear Wake Flows," Ph.D. Thesis, University of Glasgow, 1995.
- Gordeyev, S. and Thomas, F., "Coherent Structure in the Turbulent Planar Jet. Part.1 Extraction of the Proper Orthogonal Decomposition Eigenmodes and Self-similarity," *Journal of Fluid Mechanics*, Vol. 414, 2000, pp. 145-194.
- Guy, Y., McLaughlin, T. E., Albertson, J. A., "Effect of Geometric Parameter on the Velocity Output of a Synthetic Jet Actuator", AIAA Paper 2002-0126, January 2002.
- Holmes, P., Lumley, J. L., and Berkooz, G., "Turbulence, Coherent Structures, Dynamical Systems, and Symmetry," Cambridge University Press, Cambridge, 1996.
- Isidori, A., *Nonlinear Control Systems*, Springer-Verlag, 1995.
- Jang, J.-S. R., Sun, C.-T., and Mizutani, E., *Neuro-Fuzzy and Soft Computing*, PTR Prentice-Hall, 1997.
- Lumley, J., "The Structure of Inhomogeneous Turbulent Flows," *Atmospheric turbulence and wave propagation*, Nauka, Moscow, 1967, pp. 166-176.
- McGrath, S. and Shaw, L., "Active Control of Shallow Cavity Acoustic Resonance," AIAA Paper 96-1949, June 1996.
- Rossiter, J. E., "Wind Tunnel Experiments on the Flow Over Rectangular Cavities at Subsonic and Transonic Speeds," RAE Tech. Rep. 64037, 1964, and Aeronautical Research Council Reports and Memoranda No. 3438, October 1964.
- Rowley, C. W., Colonius, T., and Murray, R. M., "Dynamical Models for Control of Cavity Oscillations, AIAA Paper 2001-2126, May 2001.
- Rowley, C. W., Williams, D. R., Colonius, T., Murray, R. M., MacMartin, D. G., and Fabris, D., "Model-Based

- Control of Cavity Oscillations Part II: System Identification and Analysis,” AIAA Paper 2002-0972, January 2002.
- Rowley, C. W., “Modeling, Simulation and Control of Cavity Flow Oscillations,” Ph.D. Thesis, California Institute of Technology, 2002.
- Rowley, C. W. and Williams, D. R., “Control of Forced and Self-Sustained Oscillations in the Flow Past a Cavity,” AIAA Paper 2003-0008, January 2003.
- Samimy, M., Debiasi, M., Caraballo, E., Özbay, H., Efe, M. Ö., Yuan, X., DeBonis, J., and Myatt, J.H., Closed-Loop Active Flow Control – A Collaborative Approach,” AIAA Paper 2003-0058, January 2003.
- Sirovich, L., “Turbulence and the Dynamics of Coherent Structures,” *Quarterly of Applied Mathematics*, Vol. XLV, No. 3, 1987, pp. 561-590.
- Sirovich, L. and Rodriguez, J., “Coherent Structures and Chaos: a Model Problem,” *Phys. Letters A*. 120(5), 1987, pp. 211-214.
- Slotine, J.-J. E. and Li, W., *Applied Nonlinear Control*, Prentice-Hall, New Jersey, 1991
- Smith, B. L. and Glezer, A., “The Formation and Evolution of Synthetic Jets,” *Physics of Fluids*, Vol. 10, No. 9, 1998, pp. 2281-2297.
- Smith, D. R., Siegel, S., and McLaughlin, T., “Modeling of the Wake Behind a Circular Cylinder Undergoing Rotational Oscillation,” AIAA Paper 2002-3066, June 2002.
- Stanek, M., Sinha, N., Seiner, J., Pearce, B., and Jones, M., “High Frequency Flow Control – Suppression of Aero-Optics in Tactical Directed Energy Beam Propagation and the Birth of a New Model (Part I),” AIAA Paper 2002-2272, May 2002.
- Stanek, M. J., Raman, G., Ross, J. A., Odedra, J., Peto, J., Alvi, F., and Kibens, V., “High Frequency Acoustic Suppression – The Role of Mass Flow, The Notion of Superposition, And The Role of Inviscid Instability – A New Model (Part II),” AIAA Paper 2002-2404, June 2002.
- Toker, O. and Özbay, H., “ H_∞ Optimal and Suboptimal Controllers for Infinite Dimensional SISO Plants,” *IEEE Transactions on Automatic Control*, Vol. 40, 1995, pp. 751-755.
- Ukeiley, L., Kannepalli, C., Arunajatesan, S., and Sinha, N., “Low-Dimensional Description of Variable Density Flows” AIAA Paper 2001-0515, January 2001.
- Williams, D. R., Fabris, D., and Morrow, J., “Experiments on Controlling Multiple Acoustic Modes in Cavities,” AIAA Paper 2000-1903, June 2000.
- Williams, D. R., Rowley, C., Colonius, T., Murray, R., MacMartin, D., Fabris, D., and Albertson, J., “Model-Based Control of Cavity Oscillations – Part 1: Experiments,” AIAA Paper 2002-0971, January 2002.
- Yuan, X., Efe, M.Ö., and Özbay, H., “On Delay-Based Linear Models and Robust Control of Cavity Flows,” presented at the NSF-CNRS Workshop on Advances in Time Delay Systems, Jan. 22-24, France, 2003

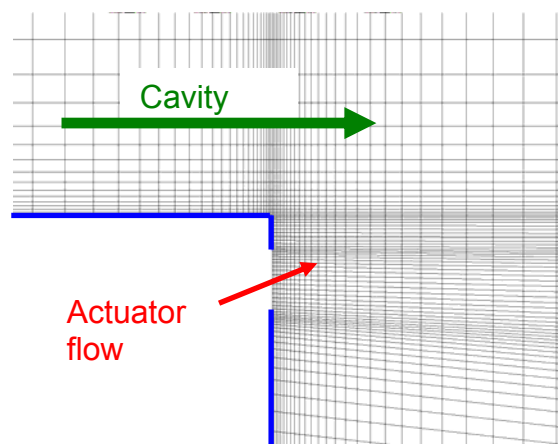


Figure 2.1: Simulation grid distribution around the actuator. The actuator outlet height is 1 mm.

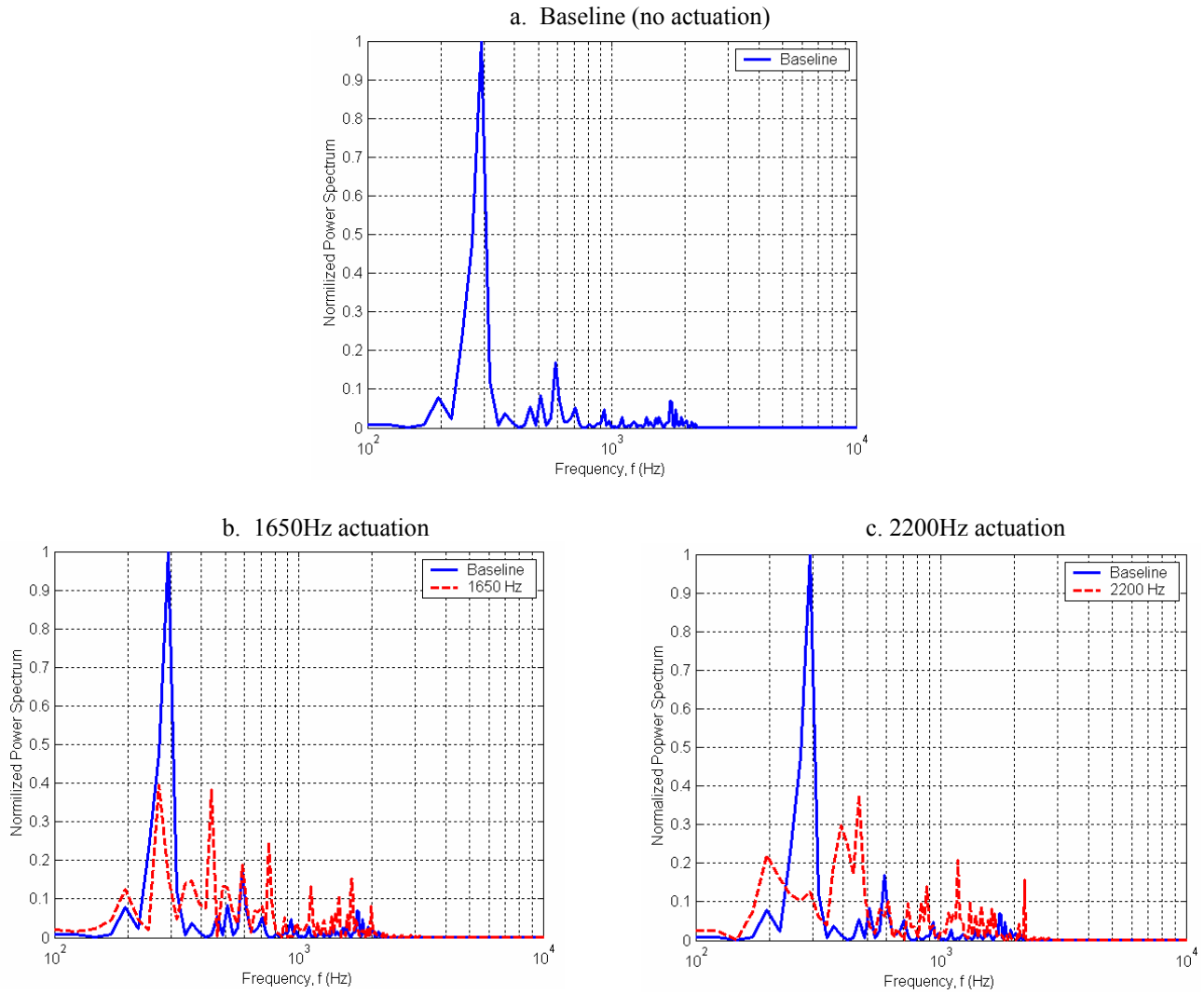


Figure 2.2: Normalized pressure spectra at the center of the cavity floor.

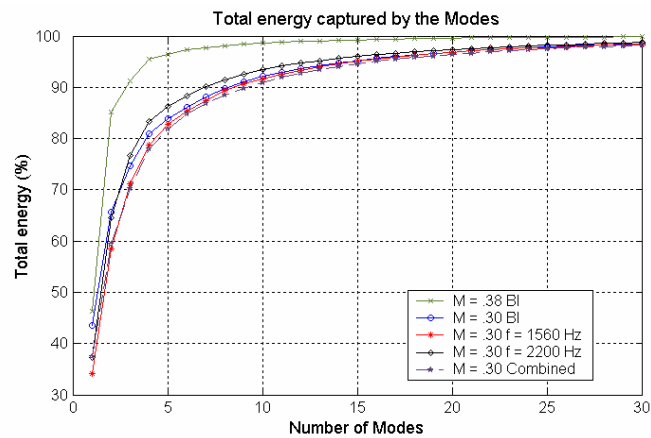


Figure 3.1: Percent of energy recovered by the POD modes in various flow/forcing cases.

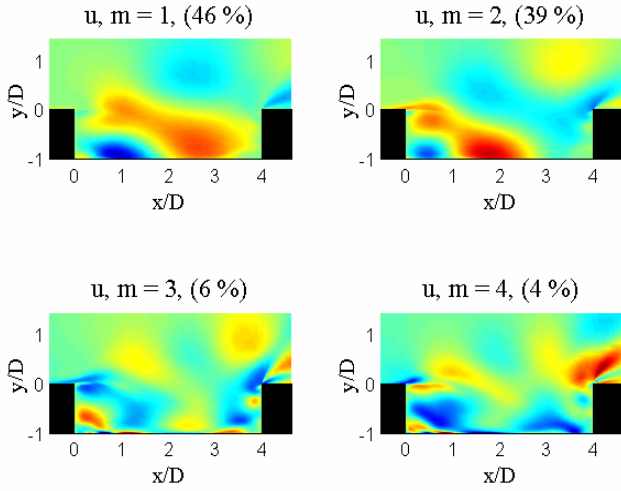


Figure 3.2: First four modes for the streamwise velocity of $M = 0.38$ baseline cavity flow.

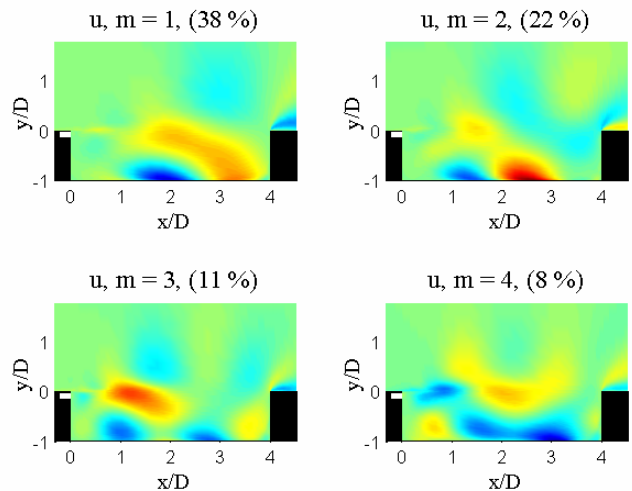


Figure 3.3: First four modes for the streamwise velocity of $M = 0.3$ baseline cavity flow.

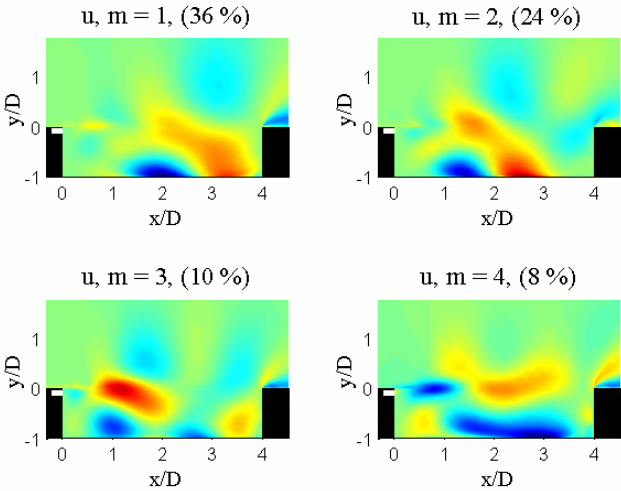


Figure 3.4: First four modes for the streamwise velocity of $M = 0.3$ cavity flow at forcing frequency of 1650 Hz.

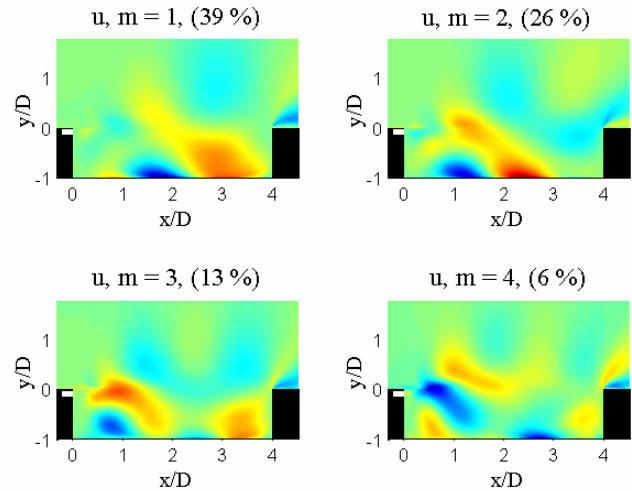


Figure 3.5: First four modes for the streamwise velocity of $M = 0.3$ cavity flow at forcing frequency of 2200 Hz.

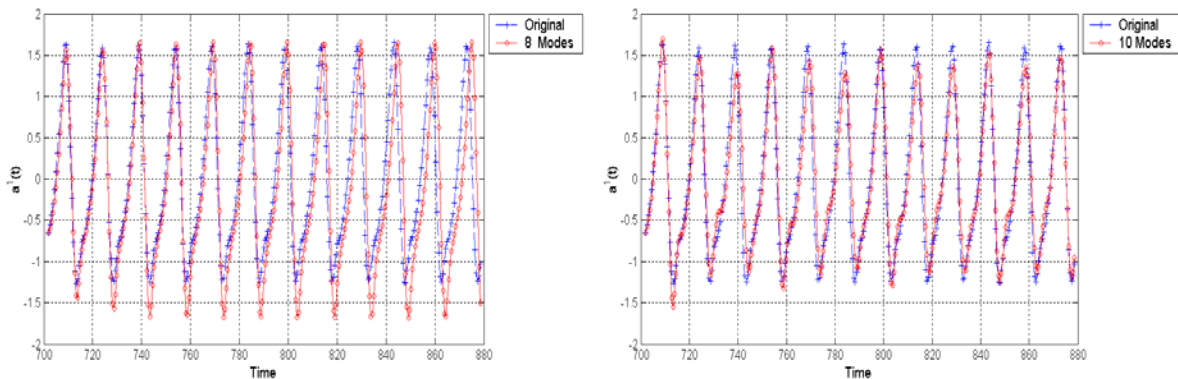


Figure 3.6: First time coefficient from the system of ODEs for $M = 0.38$ baseline cavity flow for eight and ten modes.

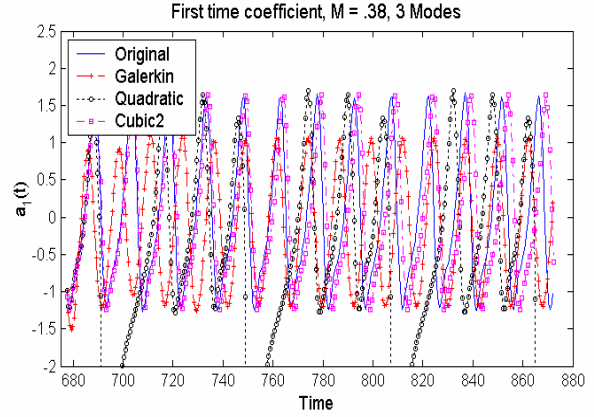
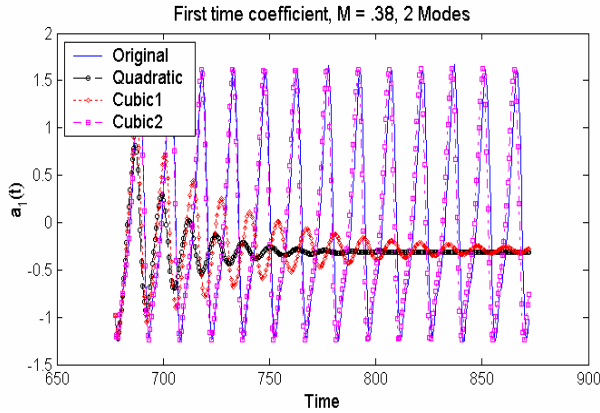


Figure 3.7: Comparison of first time coefficient obtained using Galerkin projection or least square method for $M = 0.38$ baseline cavity flow; left: two modes, right: three modes.

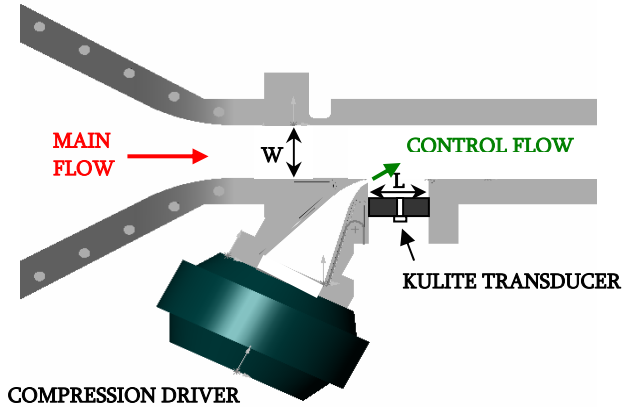


Figure 5.1: Section of the experimental facility showing the converging nozzle, the test section, the cavity, the actuator, and the placement of the Kulite transducer.

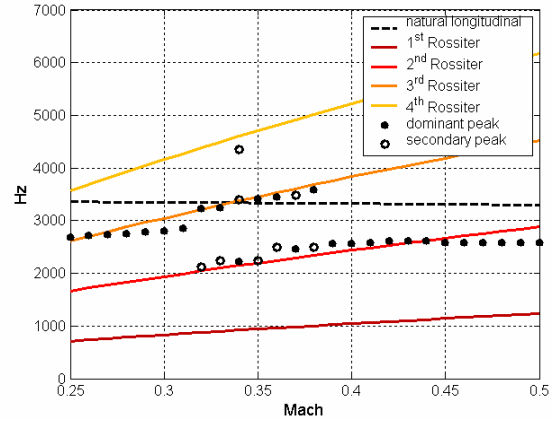


Figure 5.2: Rossiter resonant frequencies (lines), measured frequencies (dots), and cavity longitudinal mode (dashed line) as a function of the flow Mach number.

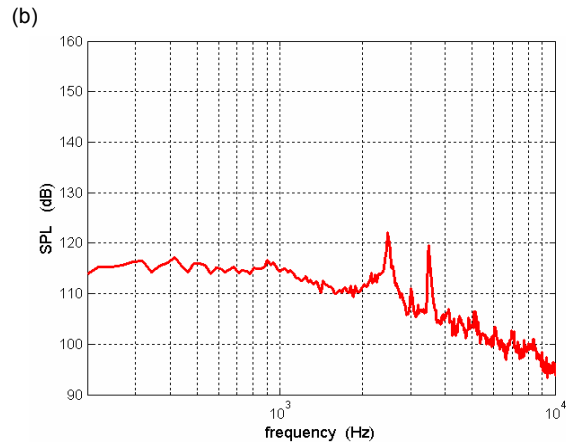
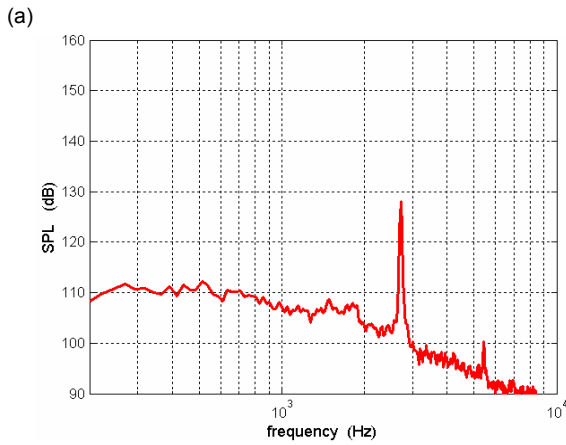


Figure 5.3: Noise spectra of cavity flow at selected Mach numbers: (a) $M = 0.26$; (b) $M = 0.37$

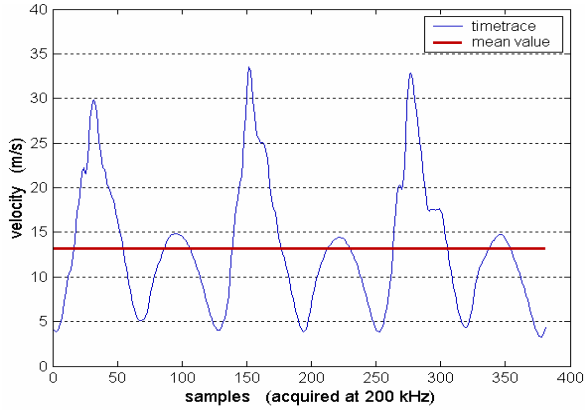


Figure 5.4: Timetrace and mean value of the velocity at exit slot for actuation at 1600 Hz and excitation $5 V_{rms}$ in absence of main flow.

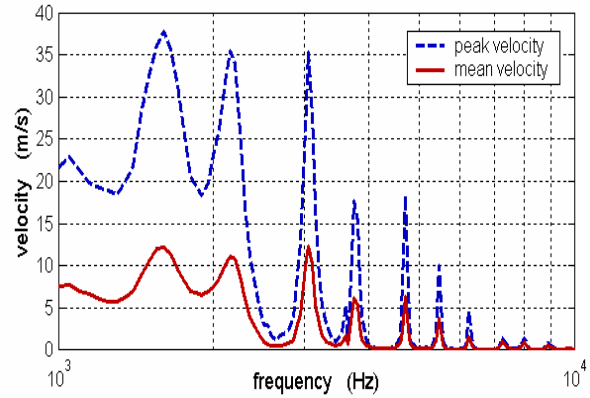


Figure 5.5: Variation of the peak and mean velocity at the exit slot as a function of the actuation frequency for excitation at $5 V_{rms}$ in absence of main flow.

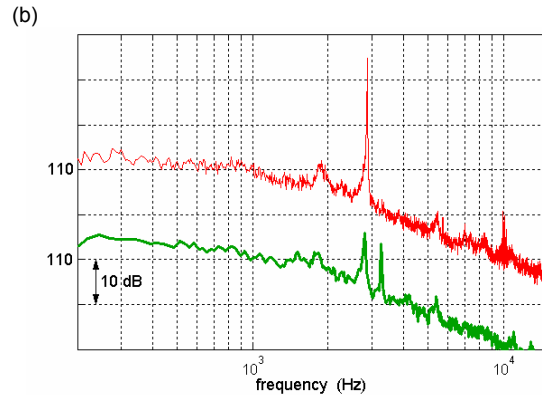
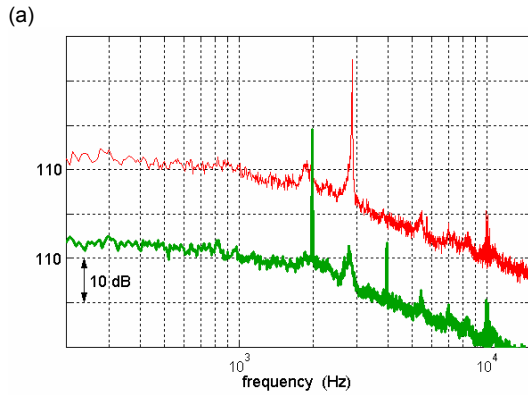


Figure 5.6: Effect of actuation frequency on Mach 0.3 flow; thin (top) line is the spectrum without actuation, thick (bottom) line with actuation at: (a) 2000 Hz; (b) 3250 Hz

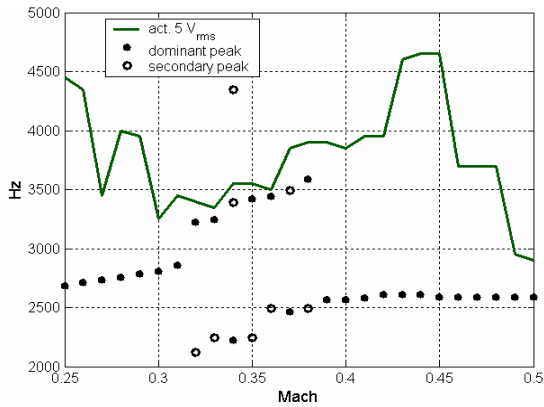


Figure 5.7: Peak frequencies and optimal frequency for their reduction as a function of the flow mach number.

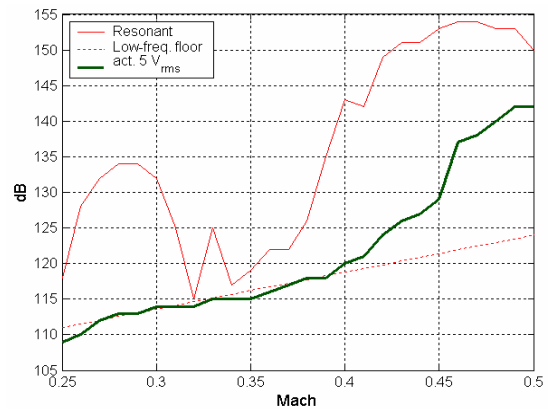


Figure 5.8: Intensity of the dominant resonant peak and of the maximum noise level at optimal frequency for peak reduction as a function of the flow Mach number.